Hinge modes and surface states in second-order topological three-dimensional quantum Hall systems induced by charge density modulation

Paweł Szumniak,[1] Daniel Loss,[2] and Jelena Klinovaja[2]

[1]*AGH University of Science and Technology, Faculty of Physics and Applied Computer Science, al. Mickiewicza 30, 30-059 Kraków, Poland*

[2]*Department of Physics, University of Basel, Klingelbergstrasse 82, 4056 Basel, Switzerland*

(Received 15 October 2019; accepted 25 August 2020; published 16 September 2020)

We consider a system of weakly coupled one-dimensional wires forming a three-dimensional stack in the presence of a spatially periodic modulation of the chemical potential along the wires, equivalent to a charge density wave (CDW). An external static magnetic field is applied parallel to the wire axes. We show that, for a certain parameter regime, due to interplay between the CDW and magnetic field, the system can support a second-order topological phase characterized by the presence of chiral quasi-1D quantum Hall effect (QHE) hinge modes. Interestingly, we demonstrate that direction of propagation of the hinge modes depends on the phase of the CDW and can be reversed only by electrical means without the need of changing the orientation of the magnetic field. Furthermore, we show that the system can also support 2D chiral surface QHE states, which can coexist with one-dimensional hinge modes, realizing a scenario of a hybrid high-order topology. Performing two-terminal transport simulations in the linear response regime, we confirm quantized QHE resistance plateaus, which are highly robust to disorder giving a clear signature of hinge and surface states.

DOI: 10.1103/PhysRevB.102.125126

I. INTRODUCTION

Over the last decade topological phases of matter have attracted considerable attention in condensed matter physics. This was triggered by the discovery of the quantum Hall effect (QHE) [1–4] with striking stability of the edge states [5]. These findings motivated a large amount of experimental and theoretical work on other topological systems such as fractional QHE [6,7], topological insulators (TIs), and superconductors (TSCs). In d-spatial dimension, the bulk of those systems is gapped while there exist topologically protected gapless states on their $(d-1)$-dimensional boundaries [8]. Very recently concepts of topological materials have been generalized to a new class of d-dimensional systems which host topologically protected edge states on $(d-n)$ dimensional boundaries, which are referred to as nth order TIs and TSCs [9–35].

In the present work, we propose a 3D system related to the QHE and analyze its transport properties, see Fig. 1. We uncover striking properties such as 1D chiral hinge modes—realizing second-order topological QHE and 2D chiral surface QHE states—present in 3D QHE [36–44], recently discovered in $ZrTe_5$ [45]. Furthermore, the studied system can host both types of states coexisting in the gap supporting a hybrid scenario with mixed higher-order topology, investigated in the context of higher-order TSCs [34,35]. Remarkably, the direction of propagation of the hinge modes can be tuned all electrically by changing the phase of the CDW potential. This extraordinary feature paves the way for an all-electrical control of the propagation direction of topological hinge modes without the need of changing the orientation of the external magnetic field, nor does it require any spin-orbit interaction. We expect that such an effect can be realized in systems where the CDW is induced by electric fields in stacked 2DEGs or stacked monolayer systems.

II. MODEL

We consider a 3D coupled-wire construction [46–58] in the presence of a uniform magnetic field applied along the wire axis, see Fig. 1. In addition, we include a CDW modulation

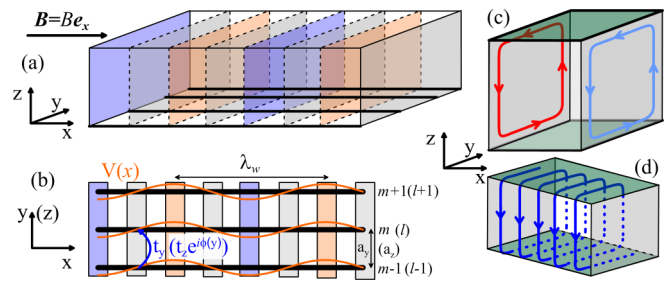

FIG. 1. (a) A 3D stack of weakly coupled wires in a magnetic field B applied along their axis. (b) The wires (thick black lines) aligned along the x axis and labeled by the indexes m (l) are weakly coupled with tunnel amplitude t_y, (t_z) in the y (z) direction. The vector potential $\mathbf{A} = By\boldsymbol{e}_z$ is chosen to be in the z direction such that the corresponding tunneling phase $\phi(y) = eBa_z y/\hbar c$ is position dependent, where a_z is the distance between neighboring wires in the z direction. In addition, there is a CDW modulation $V(x)$ [orange wavy line (b)] of the chemical potential of the wires with period λ_w. The sketch of (c) the hinge modes localized on the left (red) and right (blue) surfaces and of (d) surface states localized on all surfaces except left and right. Green areas indicated leads attached to the system for the purpose of transport studies.

along the wires [Fig. 1(b)]. Such CDWs may be induced intrinsically by electron-electron interactions [45,59–61] or by an internal superlattice structure [62,63], or extrinsically by periodically arranged gates inducing spatial modulations of the chemical potential [64,65]. The system is then described by the following tight-binding Hamiltonian,

$$H_{3D} = \sum_{n,m,l} \Big[- t_x c^\dagger_{n+1,m,l} c_{n,m,l} - t_y c^\dagger_{n,m+1,l} c_{n,m,l} - t_z e^{im\phi} c^\dagger_{n,m,l+1} c_{n,m,l} - \frac{1}{2}(V(n)+\mu) c^\dagger_{n,m,l} c_{n,m,l} + \text{H.c.} \Big], \tag{1}$$

where $c_{n,m,l}$ is the annihilation operator acting on the electron at a site (n, m, l) of the lattice with the lattice constants $a_{x,y,z}$ in the respective directions. Here, without loss of generality, the hopping matrix elements $t_{x,y,z}$ are assumed to be real. For simplicity, we consider spinless electrons in this work. A uniform magnetic field is applied in the x direction, $\boldsymbol{B} = B\boldsymbol{e}_x$, and the corresponding vector potential, $\boldsymbol{A} = By\boldsymbol{e}_z$, is chosen along the z axis, yielding the orbital Peierls phase $\phi = eBa_y a_z/\hbar c$. The chemical potential is modulated in the presence of the CDW as $V(n) = 2U_0 \cos(2k_w n a_x + \varphi)$ with the CDW amplitude $2U_0 > 0$ and the period $\lambda_w = \pi/k_w$. The angle φ is the phase of the CDW at the left end of the wire ($n = 0$). Later, to investigate transport properties of the finite 3D system, we calculate two-terminal conductance $G(E)$ [resistance $\rho(E) = 1/G(E)$] as a function of energy E using the Kwant package [66].

With this choice of the vector potential **A**, the system is translation invariant in the z direction, thus, we can introduce the momentum k_z via Fourier transformation $c_{n,m,l} = \frac{1}{\sqrt{N_z}} \sum_{k_z} c_{n,m,k_z} e^{-ilk_z a_z}$, where N_z is the number of lattice sites in the z direction. The Hamiltonian becomes diagonal in the k_z space,

$$H(k_z) = \sum_{n,m,k_z} \Big(\big[- t_x c^\dagger_{n+1,m,k_z} c_{n,m,k_z} - t_y c^\dagger_{n,m+1,k_z} c_{n,m,k_z} + \text{H.c.} \big] - c^\dagger_{n,m,k_z} c_{n,m,k_z} [\mu + V(n) + 2t_z \cos(m\phi + k_z a_z)] \Big). \tag{2}$$

As a result, the eigenfunctions of H factorize as $e^{ik_z z}\psi_{k_z}(x, y)$, with $x = na_x$, $y = ma_y$, and $z = la_z$. From now on, we focus on $\psi_{k_z}(x, y)$ and treat k_z as a parameter.

III. INGREDIENTS: CDW MODULATED WIRE AND 2D IQHE

The presence of a CDW along a single wire leads to an opening of a gap in the energy spectrum and for certain values of φ to the emergence of in-gap end states (see Fig. 2). We choose $2k_w a_x = \pi/2$ for all plots to follow. This value is consistent with the period of interaction-induced CDWs in $ZrTe_5$ material [45] that is approximately four times the lattice constant. For this choice, the system is gapped at filling factors 1/4 and 3/4. In Fig. 2(a), we plot a part of the spectrum of a finite wire (see also Appendix A) around the lowest gap (at filling factor 1/4) as a function of φ. At the special values

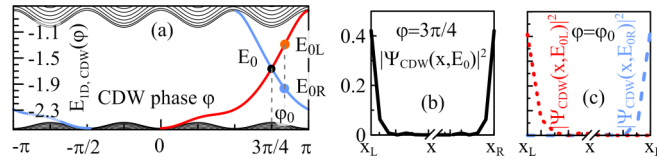

FIG. 2. (a) Energy spectrum of a single wire with CDW modulation as function of phase φ around the lowest gap at filling factor 1/4. For $\varphi = 3\pi/4$ the gap contains doubly degenerate end states at energy E_0 and for $\varphi = \varphi_0$ two nondegenerate end states at energies E_{0L} and E_{0R}. (b),(c) The corresponding probability densities $|\Psi_{\text{CDW}}(x; E)|^2$ for $E = E_0, E_{0L}, E_{0R}$ indicate that double-degenerate states at E_0 are localized at both ends of the wire, while states at energies E_{0L} and E_{0R} are localized at the left (x_L) and the right (x_R) end of the wire. Here, we choose $U_0 = 0.9t_x$, $N_x = 40$, and $2k_w a_x = \pi/2$.

$\varphi = -\pi/4, 3\pi/4$, the system has an inversion symmetry. For $\varphi = -\pi/4$, there are no states in the lowest energy gap, while for $\varphi = 3\pi/4$ two degenerate end states [localized at the both ends of the wire, see Fig. 2(b)] emerge in the gap at energy E_0 [64,65,67–76] and are weakly topologically protected by inversion symmetry [64,77,78]. If one tunes away from $\varphi = 3\pi/4$, the in-gap states split in energy. The states with $\partial E(\varphi)/\partial\varphi > 0$ [$\partial E(\varphi)/\partial\varphi < 0$] are localized at the left (right) end of the wire at x_L (x_R) as illustrated in Fig. 2(c). At other values of φ, the system is fully gapped and there are no bound states. On the other hand, electrons in a single 2D yz layer and in the presence of a perpendicular magnetic field exhibit the well-known Hofstadter spectrum [79] with chiral edge states. For illustrative purposes, we consider the simplest case with a resonant magnetic field value leading to $\phi = \pi/2$, corresponding to the QHE filling factor $\nu = 1$. (However, we emphasize that our results are valid for other values of magnetic flux with higher QHE filling factors and for other periods of the CDW potential as we show in Appendix B.) In our proposal, we combine these two mechanisms, which leads to opening of gaps and emergence of in-gap states that are exponentially localized on the hinges of the left ($x = x_L, y, z$) [($\bar{1}$, 0, 0)] and right ($x = x_R, y, z$) [(1,0,0)] surfaces, see Fig. 3. For the choice $2k_w a_x = \pi/2$, the spectrum of the 3D system is characterized by two CDW-induced gaps (at 1/4 and 3/4 filling). We take the amplitude of the CDW potential U_0 to be sufficiently large so that the 2D QHE spectrum (or at least one of the QHE gaps) fully fits inside the CDW-induced gap. This requires $U_0 \gg 4t_y$. The effects of different values of U_0 on the spectrum is discussed in Appendix B.

IV. RESULTS: HINGE MODES

A. Degenerate QHE hinge modes

First we consider the case with $\varphi = 3\pi/4$ for which a single CDW modulated wire has a spectrum with two degenerate in-gap end states at energy E_0. In this case, we find doubly degenerate copies of the 2D QHE spectrum inside the CDW-induced gap centered around E_0 [see Fig. 3(a)]. The quasi-2D QHE bulk states [green lines in Fig. 3(a)] are exponentially localized at the right and left surfaces of the system. One can see two QHE gaps ($\nu = 1$) with doubly degenerate hinge modes $E^\sigma_{LR}(k_z)$, where the index $\sigma = \circlearrowleft, \circlearrowright \equiv -1, 1$ corresponds to

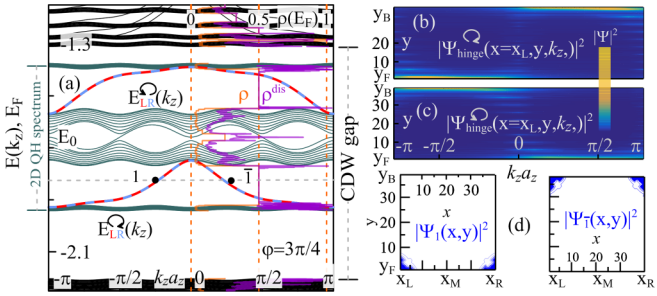

FIG. 3. (a) The spectrum of the system from Fig. 1(a) with periodic boundary conditions in the z direction around the lowest CDW-induced gap for $\varphi = 3\pi/4$. Two degenerate copies of a 2D QHE spectrum are centered around E_0 within two QHE gaps. The 2D QHE bulk bands (green) and 1D hinge modes E^{σ}_{LR} (dashed red-blue) are localized at the left and right surfaces with $\sigma =$ ↺ (1) and $\sigma =$ ↻ (−1) denoting the propagation direction of the hinge modes. The two-terminal resistance $\rho(E_F)$ for clean (orange) and disordered (purple) systems from Figs. 1(c) and 1(d) as a function of Fermi energy E_F with QHE plateaus at $\rho = \rho^{\rm dis} = 0.5[h/e^2]$ for E_F lying in the gaps hosting a pair of degenerate QHE hinge modes. (b),(c) The cross sections of the QHE hinge modes probability density $|\Psi^{\sigma}_{\rm hinge}(x = x_L, y, k_z)|^2 = |\Psi^{\sigma}_{\rm hinge}(x = x_R, y, k_z)|^2$. (d) The probability density $|\Psi_1(x, y)|^2$, $|\Psi_{\bar 1}(x, y)|^2$ for the QHE hinge modes at selected k_z points, 1 and $\bar 1$, indicated in (a). Here, we set $t_x = 1$, $t_y = 0.11t_x$, $t_z = 0.09t_x$, $U_0 = 0.9t_x$, $2k_w a_x = \pi/2$ with $N_x \times N_y(\times L_z) = 40 \times 39(\times 40)$ lattice points (for transport) and take a resonant magnetic field $\phi = 2k_F a_y = \pi/2$, corresponding to filling factor $\nu = 1$.

the direction of propagation/circulation in the yz plane for open boundary conditions in both the y and z directions. In Fig. 3(a), the presence of doubly degenerate in-gap hinge modes gives rise to quantized QHE resistance plateau at $\rho = 1/G = 0.5[h/e^2]$ for clean (orange) and disordered (purple) systems.

The hinge modes are chiral as indicated by the probability densities $|\Psi^{\sigma}_{\rm hinge}(x = x_L, y, k_z)|^2 = |\Psi^{\sigma}_{\rm hinge}(x = x_R, y, k_z)|^2$ [see Figs. 3(b) and 3(c)] and are exponentially localized at certain corners of the xy-cross section [see Fig. 3(d)]. For a finite-size system with open boundary conditions in all directions, the hinge modes circulate in the same direction on the hinges adjacent to the left and right surface of the system [as schematically illustrated in Fig. 1(c)], in analogy to unidirectional edge states [80–82].

B. Hinge mode regimes

In order to systematize the regimes in which hinge modes exist, we plot the spectrum as a function of φ for fixed $k_z = 0$ or $\pi/2$ in Fig. 4. The QHE gaps marked by pale orange (green) host only one hinge mode with the counterclockwise $\sigma =$ ↺ (clockwise $\sigma =$ ↻) direction of propagation. The dark orange (green) regions around $\varphi = 3\pi/4$ correspond to a scenario where QHE gaps of each QHE copy overlap thus host two hinge modes (one at the left and one at the right surface) with the same positive (negative) σ. For $\varphi = 3\pi/4$, the QHE gaps of each QHE copy fully overlap. If one deviates from $\varphi = 3\pi/4$, the degeneracy of the QHE spectrum is lifted. Each of the 2D QHE copies is now shifted in energy, either

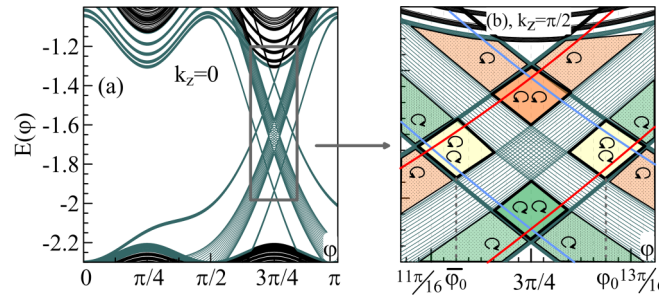

FIG. 4. (a) Spectrum of the 3D system from Fig. 1(a) around the CDW-induced gap as a function of φ for $k_z = 0$. The interesting part, where the QHE spectra of states localized at the left and right surfaces cross and overlap, is marked by a gray rectangle and zoomed in on panel (b) for $k_z a_z = \pi/2$. The pale orange (green) color denotes QHE gaps with a single hinge mode characterized by counterclockwise $\sigma = 1 =$ ↺ (clockwise $\sigma = -1 =$ ↻) direction of propagation. The dark orange (green) areas denotes QHE gaps with a pair of chiral unidirectional QHE hinge modes with $\sigma = 1$ ($\sigma = -1$) localized at the left and right surfaces. The yellow area denotes a scenario with a pair of in-gap hinge modes propagating in opposite directions on the left and right surface. The solid red (blue) lines correspond to hinge modes localized at hinges adjacent to the left (right) surface.

up or down, and corresponding states are localized at the left or right surfaces, consistent with the picture emerging from 1D CDW-induced end states in Fig. 2. The hinge modes are circulating again in the same directions on each surface (see Appendix A). Moreover, further increase of φ leads to closing of the QHE gaps in such a way that the gap of one of the QHE copies overlaps in energy with the 2D QHE bulk states of the other copy localized at the opposite surface. Interestingly, there is a region around $\varphi = \varphi_0$ and $\bar\varphi_0$ (marked by yellow rectangles), where the hinge modes of opposite σ coexist (see Fig. 5). The system hosts hinge modes propagating in opposite directions on hinges adjacent to the left and right surface. The

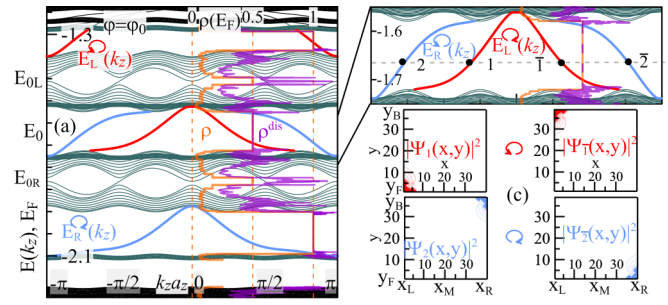

FIG. 5. Same as in Fig. 3 but for $\varphi = \varphi_0$. The two degenerate copies of the bulk QHE spectrum from Fig. 3 are split in energies such that each one is centered around E_{0R} and E_{0L}, respectively. The part of the QHE spectrum around E_{0R} (E_{0L}) corresponds to states localized on left (right) surface. Interestingly, for the chosen CDW phase $\varphi = \varphi_0$, in the gap around E_0 we find a pair of chiral hinge modes that propagate in the opposite directions on the left and the right surface. We can see stable quantized resistance plateaus at $\rho = 0.5[h/e^2]$ ($\rho = 1[h/e^2]$) for the energies lying in the gap which hosts two (one) hinge modes for clean (orange) and disordered (purple) system. (c) The corresponding wave function probability $\Psi_{1,\bar 1,2,\bar 2}$ for k_z momenta marked by 1, $\bar 1$, 2, $\bar 2$ points on panel (a).

direction of propagation can be reversed by changing φ from a region around φ_0 to one close to $\bar{\varphi}_0$ without the need of changing μ. The change of propagation direction of the hinge states is due to the sign change of the effective mass of carriers. The overlap of the QHE gaps is maximal for $\varphi = \varphi_0$ and $\bar{\varphi}_0$. The edge states localized on the hinges adjacent to the left (right) surfaces are marked by red (blue) solid lines. Further increase of φ away from $\varphi = 3\pi/4$ leads to the separation in energy of these two QHE copies. We also checked numerically that hinge modes are robust against moderate static disorder (as shown in Appendix B), however, we note that for the special case of $\varphi = 3\pi/4$ the disorder lifts the degeneracy of the hinge modes on the left and right surfaces. Importantly, we note that the gaps hosting hinge modes are true bulk gaps and are opened for arbitrary large system size ($N_x, N_y, N_z \to \infty$).

V. 2D QHE SURFACE STATES: 3D QHE AND HYBRID SCENARIO

Another striking feature of the proposed setup is the fact that it can support a 3D QHE with 2D chiral surface states. This effect looks rather similar to one observed in recent experiments [45] in which an interplay of interaction-induced CDW and magnetic field lead to 3D QHE. Here, we also discuss a hybrid scenario with mixed high-order topology [34], in which the 2D QHE chiral surface states can coexist in the gap with the 1D QHE hinge modes.

A. Bulk system

Let us first consider a case where gaps hosting 2D QHE surface states supporting 3D QHE are opened for arbitrary large N_x (true bulk system). We demonstrate such a scenario in Fig. 6. One can see two gaps (marked by yellow area) hosting 2D QHE chiral surface states (green) $E^{\sigma}_{\text{surf}}(k_z)$ with $\sigma = \circlearrowleft, \circlearrowright$. We choose system parameters ($t_y = 0.31, t_z = 0.21, U_0 = 0.9t_x, 2k_w a_x = \pi/2$) so the "upper" gap hosts 2D surface states $E^{\circlearrowleft}_{\text{surf}}(k_z)$ and doubly degenerate hinge modes $E^{\circlearrowleft}_{LK}(k_z)$ (red-blue) which propagates in the opposite direction. In this regime system realizes hybrid high-order topology. For the chosen parameters ($2k_w a_x = \pi/2$ and $\phi = \pi/2$) one can easily diagonalize the Hamiltonian with periodic boundary conditions being imposed in all three spatial dimensions (see Appendix C for details). This allows us to calculate the spectrum $E(\mathbf{k})$ for the 3D bulk system from Fig. 1 along high symmetry points in the 3D Brillouin zone [see brown curve in Fig. 6(a)] from which one can clearly see that the bulk 3D QHE gaps are independent of the system size. The presence of in-gap modes manifests in quantized QHE resistance plateaus at $\rho = 1/11[h/e^2]$ ($\rho = 1/9[h/e^2]$) for Fermi energy lying in the gaps which hosts both surface states and hinge modes (only surface states). Since in the hybrid scenario surface states and hinge modes propagates in the opposite directions this allows for backscattering at the hinges for disordered system. Thus in disordered hybrid regime the corresponding conductance is reduced and the QHE plateau is not perfectly flat [see G^{dis_1} and G^{dis_2} plots in Fig. 6(c)]. For the Fermi energies E_F lying in the gap hosting only surface states, the conductance plateau is perfectly flat even in the presence of strong disorder [see G^{dis_1} and G^{dis_2} plots in Fig. 6(c′)].

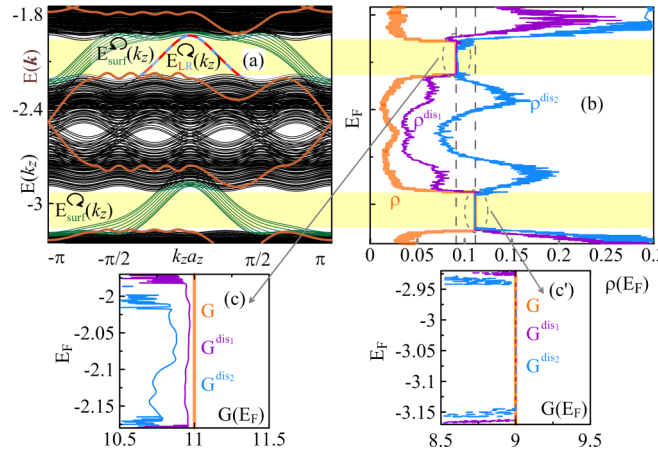

FIG. 6. (a) Spectrum of the 3D system from Fig. 1(a) with the periodic boundary conditions in the z direction around the lowest in energy 3D QHE gaps (yellow area) as a function of k_z for $\varphi = 3\pi/4$. The parameters have been chosen so that the lower in energy gap hosts exclusively chiral QHE surface states $E^{\circlearrowleft}_{\text{surf}}(k_z)$ propagating in clockwise direction, while the upper gap hosts chiral QHE surface states $E^{\circlearrowright}_{\text{surf}}(k_z)$ propagating in counterclockwise direction and pair of degenerate hinge modes $E^{\circlearrowleft}_{LK}(k_z)$ propagating in clockwise direction realizing hybrid high-order topology. The spectrum of the 3D system E(**k**) along high symmetry **k** points in 3D Brillouin zone (upper horizontal axis) with periodic boundary conditions in all the directions (brown) demonstrates the bulk character of the 3D QHE gaps. On panel (b), we plot two terminal resistance $\rho(E_F)$ for clean (orange line) and disordered system $\rho^{\text{dis}}(E_F)$ and $\rho^{\text{dis}_2}(E_F)$ (purple and blue). One can clearly see quantized QHE resistance plateaus at $\rho = 1/11[h/e^2]$ ($\rho = 1/9[h/e^2]$) for Fermi energies E_F lying in the upper (lower) gap. (c) Interestingly, in the presence of disorder for in-gap energies, conductance is reduced and not perfectly quantized for hybrid scenario with coexisting counterpropagating surface and hinge modes. (c′) This is not the case for E_F lying in the lower gap which hosts only surface modes and results in perfectly quantized conductance at $G(E_F) = G^{\text{dis}_1} = G^{\text{dis}_2} = 9[e^2/h]$ even in the presence of strong disorder. Here, we set $t_y = 0.31$, $t_z = 0.21$, $U_0 = 0.9t_x$, $2k_w a_x = \pi/2$ with $N_x \times N_y (\times N_z) = 40 \times 39 (\times 40)$ lattice points (for transport simulations) and take the resonant value for the magnetic field $\phi = \pi/2$.

B. Finite size system: Finite number of coupled layers

On the other hand one can imagine a system composed only of a finite number of coupled yz layers stacked in the x direction. In such a case for certain regime of system parameters one can interestingly notice series of small gaps around the upper edge of the CDW induced gap [see Fig. 3(a) and Appendix A]. Such gaps are opened by an interplay between magnetic field and CDW and also finite size effects (finite N_x—finite number of coupled yz layers) [83–85]. Moreover these gaps hosts 2D QHE chiral surface states supporting 3D QHE. Here we can also achieve hybrid high order topology, e.g., by pushing the 3D bulk spectrum into 2D QHE spectrum by reducing U_0 or vice versa by pushing the 2D QHE spectrum into 3D bulk spectrum by increasing t_y (see Appendix B for details). In Fig. 7, we show a part of the spectrum of the 3D system in which one can see a pair of the chiral QHE surface states localized at the front (x, y_F, z)

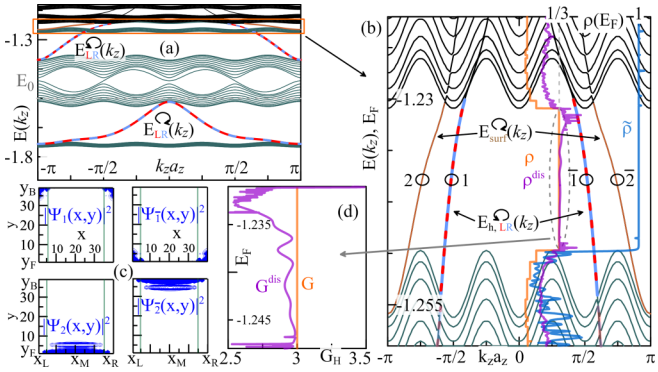

FIG. 7. (a) Same as in Fig. 3(a) but for smaller $U_0 = 0.7t$. (b) The zoomed-in part of the spectrum [marked by orange rectangle on (a)] contains the gap in which doubly degenerate chiral QHE hinge modes $E_{h,\,LR}(k_z)$ and nondegenerate QHE chiral surface states $E_{surf}(k_z)$ coexist. The resistance with quantized plateaus at $\rho = \rho^{dis} = 1/3[h/e^2]$ for clean (orange) and disordered (purple) systems and for the system with 'truncated' leads [green lines on (c)] so that only surface modes contribute to transport with resistance plateau at $\tilde{\rho} = 1[h/e^2]$ (blue). (c) The corresponding probability density $|\Psi_j(x, y, k_z^{fixed})|^2$ for fixed k_z denoted by $j = 1, \bar{1}, 2, \bar{2}$ which shows chiral character of the states. (d) Zoom of the plateau region from (b) with conductance which shows how the presence of disorder affects conductance $G^{dis} \approx 3[e^2/h]$ in a hybrid regime.

and back (x, y_B, z) surfaces and propagating in the z direction. [For the open boundary conditions along the z axis, the 2D QHE chiral surface states are circulating on all surfaces except the left and right one as sketched in Fig. 1(d).] Interestingly, we can also find coexisting pairs of doubly degenerate chiral QHE hinge modes localized at the corners of the finite xy plane and propagating in the z direction. For clean systems (without disorder) coexisting states result in resistance plateau at $\rho = 1/3[h/e^2]$ [see orange line in Fig. 7(b)]. Since the hinge modes propagate in the opposite direction to the surface states one can expect backscattering at the corners in the presence of disorder which results in resistance plateaus ρ^{dis} not being perfectly flat [conductance G^{dis} is reduced see Fig. 7(d)], which is not the case for gaps hosting exclusively hinge or surface modes. To distinguish between the two types of states we propose a setup with leads not covering corners as marked by green lines in Fig. 7(c). The corresponding resistance is equal to $\tilde{\rho} = 1[h/e^2]$ since only one surface state gives contribution to the conductance with no contribution from hinge modes. For the gap hosting only hinge modes the corresponding conductance is zero.

VI. SUMMARY

We have proposed a system which can support second-order topological QHE phases with hinge modes, 3D QHE with surface states, and a hybrid topology with both types of states. Quite remarkably, the direction of propagation of the hinge modes can be switched all electrically by tuning the phase of the CDW. We found clear and robust signatures of hinge and surface states in transport studies which show quantized resistance plateaus. This prediction is directly amenable to experimental tests. We propose that our predictions can be tested in semiconducting nanowires with CDW modulations, heterostructures forming a superlattice of 2DEGs with electrically tunable chemical potentials [62,63], organic conductors [86], systems with intrinsic CDW order, e.g., $ZrTe_5$ [45],

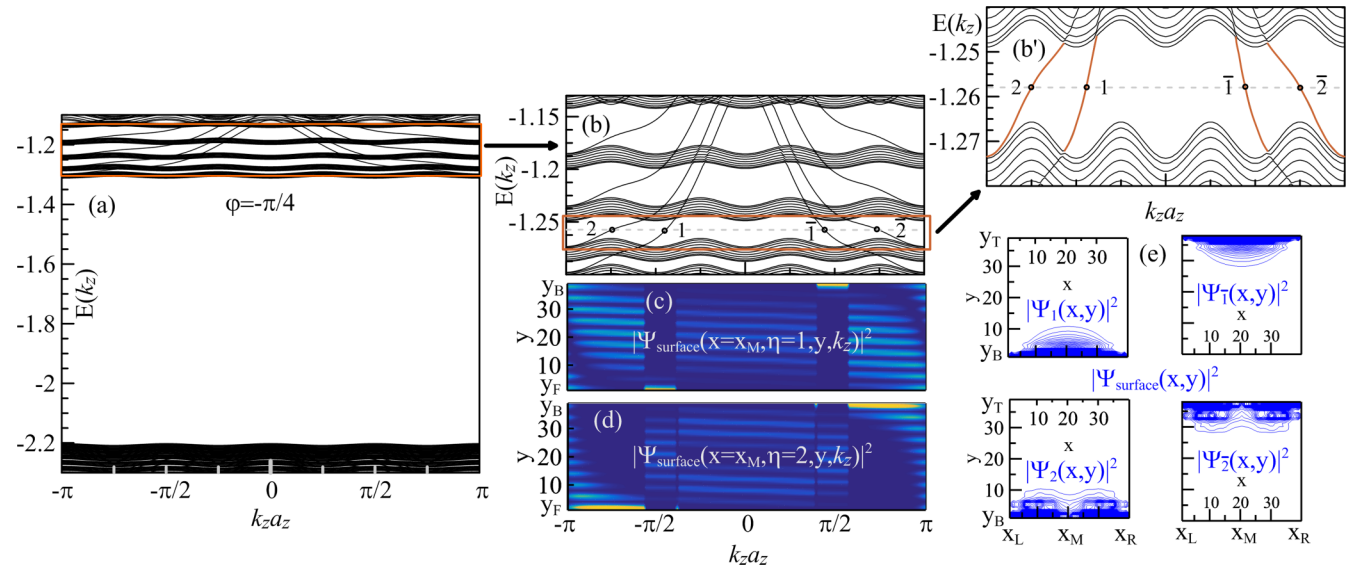

FIG. 8. (a) Spectrum of the 3D system from Fig. 1(a) from the main text with the periodic boundary conditions in the z direction around the lowest in energy CDW induced gap as a function of k_z for $\varphi = -\pi/4$. The zoom of upper edge of CDW gap is plotted in panel (b) and further zoom of one of the gaps in (b′). The color maps (c,d) shows probability density $|\Psi_{surface}(x = x_M, y, k_z)|^2$ for the first and second QHE surface mode hosted in the gap marked by the brown rectangle and further zoomed in (b′). The probability density $|\Psi_{surface}(x, y, k_z^{fixed})|^2$ for the first ($\eta = 1$) and second mode ($\eta = 2$) of the QHE chiral surface states [selected k_z^{fixed} points: $1, \bar{1}, 2, \bar{2}$ from panels (b), (b′) is represented on panel (e)]. Here, we set $t_y = 0.11$, $t_z = 0.09$, $U_0 = 0.9t_x$, $2k_w a_x = \pi/2$ with $N_x \times N_y = 40 \times 39$ lattice points and take the resonant value for the magnetic field $\phi = \pi/2$.

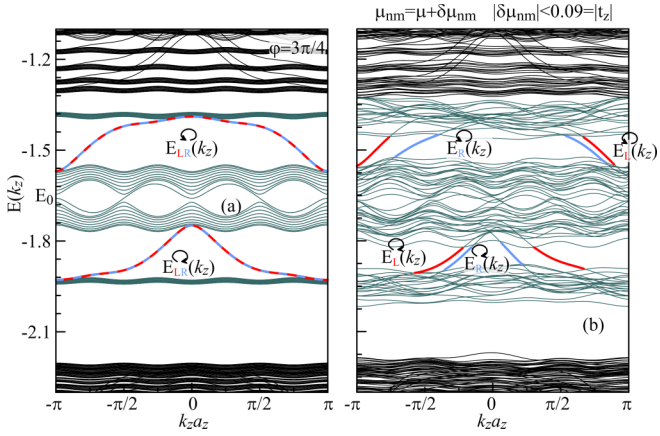

FIG. 9. Spectrum of the 3D system from Fig. 1(a) of the main text with periodic boundary conditions in the z direction around the energetically lowest CDW-induced gap as a function of k_z for $\varphi = 3\pi/4$: (a) without disorder and (b) in the presence of onsite static disorder corresponding to a uniformly fluctuating chemical potential in the range of the QHE gap $|\delta\mu_{n,m}| \leqslant 0.09 = |t_z|$. Despite the fact that the bulk gap gets smaller, the hinge modes are clearly present in the spectrum.

as well as optical lattices [87–89] or photonic crystals [90]. Finally, we expect that the CDW mechanism uncovered here will also give rise to hinge modes in other 3D topological systems composed of stacked CDW-modulated layers.

ACKNOWLEDGMENTS

We acknowledge support within POIR.04.04.00-00-5CE6/18 project carried out within the HOMING programme of the Foundation for Polish Science co-financed by the European Union under the European Regional Development Fund, Swiss National Science Foundation, and NCCR QSIT. This project received funding from the European Unions Horizon 2020 research and innovation program (ERC Starting Grant, Grant agreement No. 757725). The calculations were performed on PL-Grid Infrastructure.

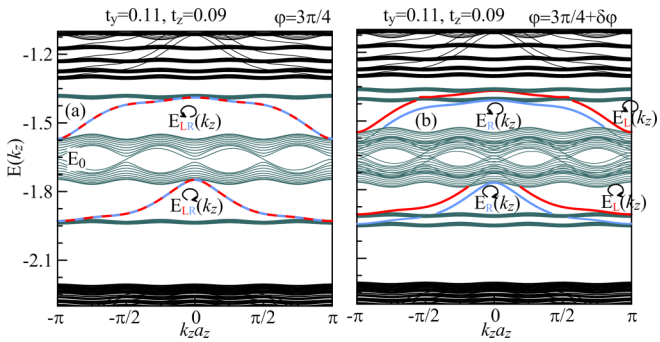

FIG. 10. Spectrum of the 3D system from Fig. 1(a) of the main text with periodic boundary conditions in the z direction around the energetically lowest CDW-induced gap as a function of k_z for (a) $\varphi = 3\pi/4$ and (b) $\varphi = 3\pi/4 + \delta\varphi$. One can clearly see in panel (b) that by moving away from $\varphi = 3\pi/4$, e.g., for $\varphi = 3\pi/4 + \delta\varphi$, the degeneracy of the two QHE spectrum copies is lifted, which results in splitting in energy of the hinge modes and bulk bands belonging to two different surfaces. Now, the QHE gaps are reduced and host two hinge modes localized on the left (red curve) and right (blue curve) surfaces which corresponds to the regimes marked by dark green and orange on Fig. 4(b) of the main text.

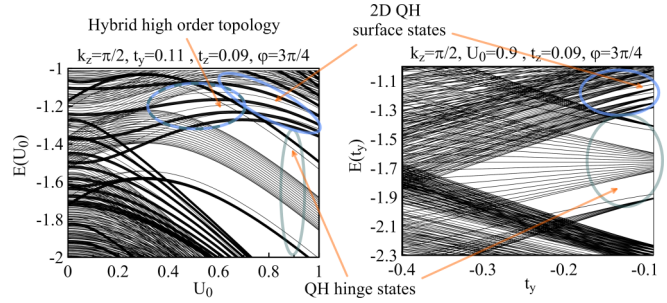

FIG. 11. Cross section of the spectrum of the 3D system from Fig. 1(a) of the main text with periodic boundary conditions in the z direction as a function of (a) U_0 and (b) t_y for fixed $\varphi = 3\pi/4$, $k_z = \pi/2$, $t_z = 0.09$, and (a) $t_y = 0.11$, (b) $U_0 = 0.9$. The interesting regimes are marked schematically by ovals. For $U_0 \gtrsim 0.8$, the part of the spectrum with hinge modes is well separated from one with QHE surface states. If U_0 is decreased, the 2D QHE spectrum with the QHE gap hosting quasi-1D hinge modes is pushed into the 3D bulk states and starts to overlap with gaps hosting 2D QHE chiral surface states. In such a regime, the scenario with a hybrid topology is realized. Further decrease of U_0 below $U_0 \lesssim 0.4$ leads to an emergence of another region with mixed higher-order topology. On the other hand, when $|t_y|$ is increased, the QHE hinge modes start to hybridize with the QHE surface states. However, in this case, the bulk states mask them, making them undetectable in transport experiments.

APPENDIX A: CHIRAL SURFACE STATES IN 3D CDW MODULATED QHE SYSTEM

Finite system in the x direction: Finite number of coupled layers

In this section, we focus on the special case with $\varphi = -\pi/4$. For this choice of parameter, there are no states in the CDW gap. However, interestingly, we can notice [see Fig. 8(b)] that the part of the spectrum around the upper edge of the CDW-induced gap (marked with the orange rectangular) contains gaps that host chiral 2D QHE surface states. This happens also for other values of φ. Such 2D QHE surface states are propagating in "$+z$" and "$-z$" direction and are localized, respectively, on the front $(x, y = y_F, z)$ and back $(x, y = y_B, z)$ surfaces [see Fig. 8(e)]. We observe a series of small gaps in which one can find from one up to four 2D QHE chiral surface states. This gaps are opened due to the interplay of the CDW and the magnetic field as well as finite size effects in the x direction play a role [83–85,91]. We assume that the system is composed of $N_x = 40$ coupled layers and find numerically that there are gaps hosting QHE surface states. However, for larger N_x, such gaps eventually get closed and QHE surface modes are masked by the bulk states reminding a behavior of bound states in continuum [92,93]. This makes them undetectable in transport experiments. The size of these gaps does not depend on the CDW phase φ, however, their

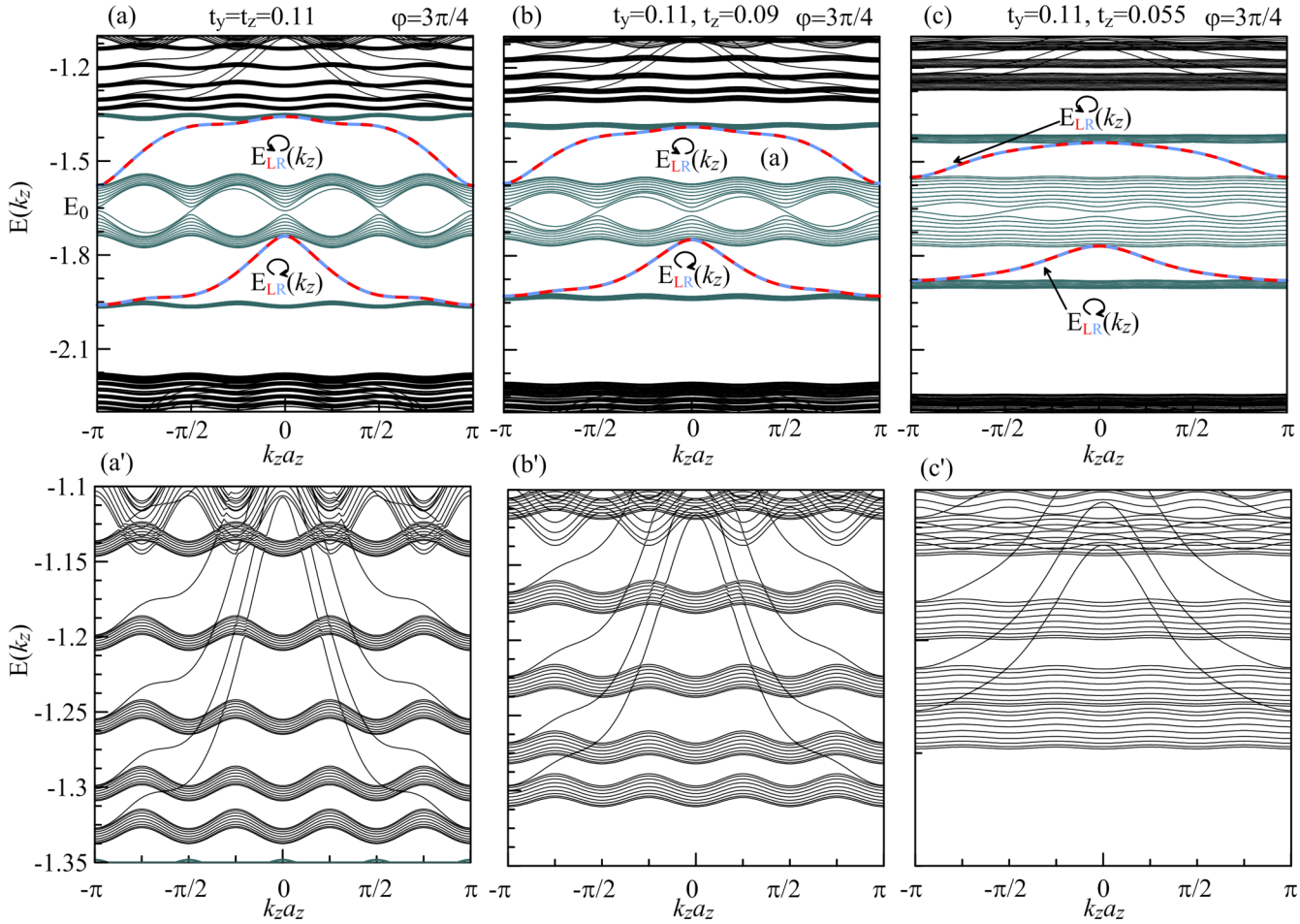

FIG. 12. Spectrum of the 3D system from Fig. 1(a) of the main text with periodic boundary conditions in the z direction around the energetically lowest CDW-induced gap as a function of k_z for $\varphi = 3\pi/4$ (a) for isotropic hopping in the yz plane with $t_y = t_z = 0.11$, (b) for a slightly anisotropic case like in the main text with $t_y = 0.11$, $t_z = 0.09$, and (c) for a highly anisotropic case with $t_y = t_z/2 = 0.055$. The lower panels (a′)–(c′) show the zoomed-in part of the spectrum with the 3D QHE gaps hosting nondegenerate 2D QHE chiral surface states. One can clearly see that decreasing t_z results in flattening of the bulk bands and in reducing the size of the gaps. Moreover, for $|t_y| \gg |t_z|$, (c) the chiral QHE hinge modes and (c′) chiral QHE surface states have a cosinelike shape.

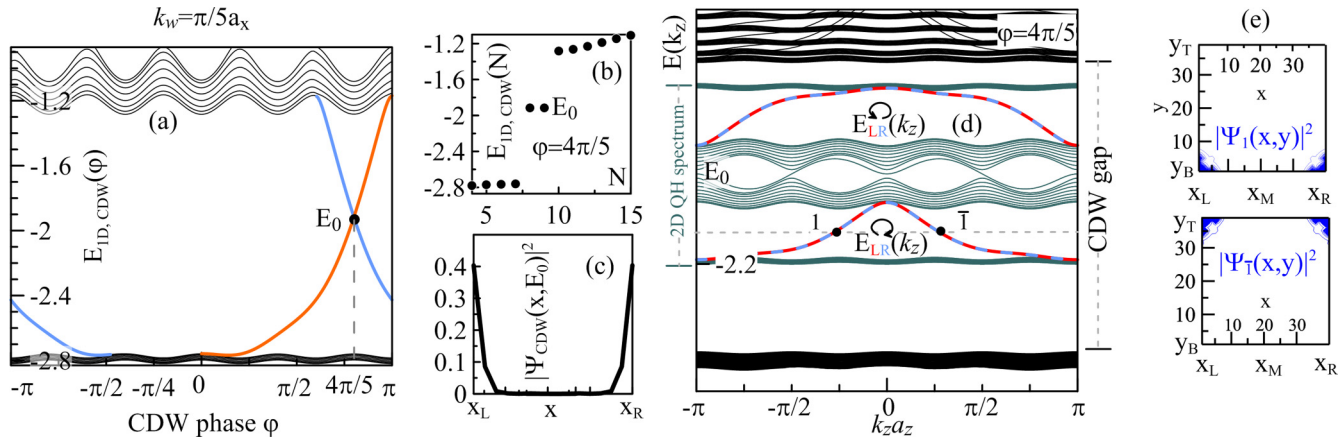

FIG. 13. (a)–(d) The same as in Figs. 2(a), 2(b) and 2(d) of the main text but for a different periodicity of the CDW potential, i.e., $k_w = \pi/5a_x$. In this case, the system has an inversion symmetry for $\varphi = 4\pi/5$ and supports doubly degenerate hinge modes in the same way as we presented in Figs. 3(a) and 3(d) of the main text.

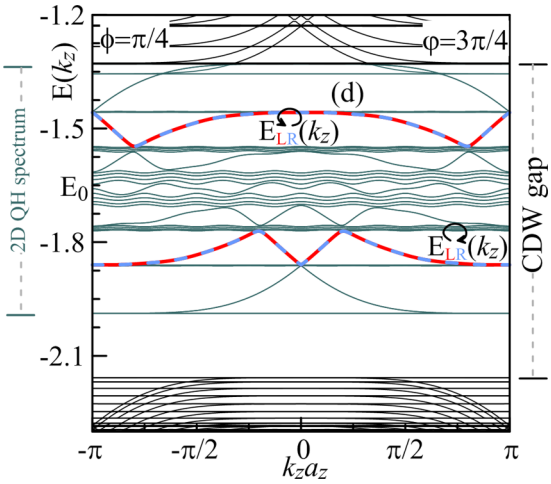

FIG. 14. Spectrum of the 3D system shown in Fig. 1(a) of the main text with periodic boundary conditions in the z direction around the energetically lowest CDW-induced gap as a function of k_z for $\varphi = 3\pi/4$—same as Fig. 3(a) of the main text but for the filling factor $\nu = 2$ with $\phi = \pi/4$. The corresponding doubly degenerate hinge modes $E^{\sigma}_{LR}(k_z)$ are marked by the red/blue dashed lines.

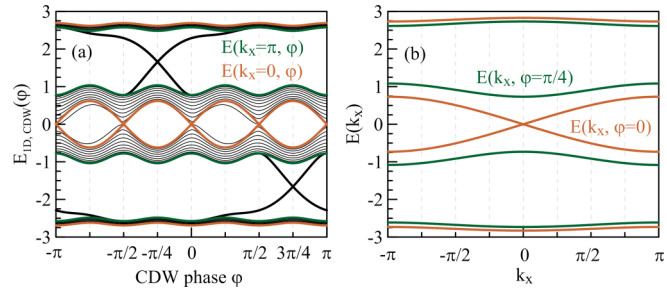

FIG. 15. Spectrum of the 1D CDW modulated wire with periodic boundary conditions described by Hamiltonian H^{1D}_{CDW}. (a) The spectrum $E(k_x, \varphi)$ as a function of CDW phase φ for fixed $k_x = 0$ (brown line) and $k_x = \pi$ (green line). (b) The spectrum $E(k_x, \varphi)$ as a function of CDW phase φ for fixed $\varphi = 0$ (brown line) and $\varphi = \pi/4$ (green line). For comparison, we also plot the spectrum of the finite-size system (see Fig. 2 main text) in panel (a) and marked it by black lines with end states denoted by thick ones. We can see perfect agreement between the gaps and position of the bulk states in the open and closed systems. The parameters are the same as in the main text, $t_x = 1$, $U_0 = 0.9$, $k_w = \pi/4$, and $N_x = 40$. We checked numerically for the finite size system that the increase of N_x leads to the increase of the number of bulk bands which lay in energy between $E(k_x = \pi, \varphi)$ and $E(k_x = \pi, \varphi)$ bands obtained for the periodic system. However, the size of the CDW induced gap remains unchanged.

position does. In the area between the gaps, the surface QHE states hybridize with the 3D bulk states. From Figs. 8(c) and 8(d), one can conclude that surface modes are chiral, i.e., for the case of periodic boundary conditions in the z direction, the 2D QHE states with $\partial E(k_z)/\partial k_z > 0$ [$\partial E(k_z)/\partial k_z < 0$] are localized at the front (back) surface.

APPENDIX B: STABILITY

Here, we study the stability of the hinge modes in the presence of disorder. We also demonstrate that the hinge modes are present in the spectrum for a wide range of system parameters.

1. Disorder

First, we investigate the effects of disorder on the stability of the hinge modes. Again, we consider static disorder—random onsite fluctuations in the chemical potential of the order of the QHE gap size: $|\delta\mu_{n,m}| \leqslant 0.09 = |t_z|$. In the presented case, for computational purposes, disorder is translationally invariant in the z direction, $\delta\mu_{n,m}(k_z) = \delta\mu_{n,m}$. One can see (Fig. 9) that bulk bands are strongly affected and the QHE gaps are reduced with respect to the clean system, however, there is still a region of k_z values for which hinge modes exist in the gap. One can also notice that disorder lifts the accidental degeneracy between left and right surfaces. Interestingly, the hinge modes are quite stable even though they exist in gaps much smaller than the fluctuations of the chemical potential.

2. Chiral hinge modes: Lifting degeneracy between right and left surfaces

Here, we show an example of a regime where there are two nondegenerate hinge modes in the gap (see Fig. 10). This scenario is realized for φ around $\varphi = 3\pi/4$, i.e., $\varphi = 3\pi/4 + \delta\varphi$ [in the region marked by the dark green and orange in Fig. 4(b) of the main text]. In this case, the degeneracy is lifted, the QHE gap is reduced, and hinge modes that are localized on the left and the right surfaces are split in energy. Furthermore, there are two more gaps that emerge in the spectrum which host a single QHE hinge mode on one of the surfaces [see pale orange and green areas in Fig. 4(b) of the main text] (Fig. 10).

3. Spectrum dependence on U_0 and t_y

We can see that for $U_0 \gtrsim 0.8$ the part of the spectrum with QHE hinge states is well separated from QHE surface states. By decreasing U_0, one can see that the upper QHE gap with quasi-1D hinge states starts to overlap with gaps hosting 2D QHE surface states. In this case, the scenario with hybrid topology is realized. Further decrease of U_0 below $U_0 \lesssim 0.4$ leads to the emergence of another region with mixed high order topology. In the left panel of Fig. 11, we explore the spectrum as a function of t_y with other parameters being fixed: $\varphi = 3\pi/4$, $k_z = \pi/2$, $t_z = 0.09$, and $U_0 = 0.9$. As $|t_y|$ is increased, QHE hinge states starts to hybridize with the QHE surface states. However, in this case, the 3D bulk states mask both states, making them undetectable in transport experiments.

4. Isotropic and anisotropic system in the yz plane

Here, we analyze effects of anisotropy in the hopping amplitude in the yz plane. To be specific, we consider the case with $t_y = t_z = 0.11$; $t_y = 0.11, t_z = 0.09$, and $t_y = t_z/2 = 0.055$. We can notice that decreasing t_z with respect to t_y causes flattening of the bulk bands. The dispersion relation of the hinge modes in the strongly anisotropic limit has a

cosinelike shape (see Fig. 12), which can be derived from the linearized model [60,94].

5. Different periodicity of the CDW: $k_w = \pi/5a_x$

The single CDW-modulated wire supports end states for different values of the period. Here, we consider an example with $2k_w a_x = 2\pi/5$, for which one obtains a pair of degenerate end states for the CDW phase equal to $\varphi = 4\pi/5$, see Figs. 13(a)–13(c). In this case, for the 3D CDW-modulated system shown in Fig. 1 of the main text, one observes a similar behavior of the hinge modes [see Figs. 13(d) and 13(e)] as obtained before in the main text for $2k_w a_x = \pi/2$ and $\varphi = 3\pi/4$ [see Figs. 3(a) and 3(d) of the main text].

6. Higher QHE filling factors

As one can expect the hinge modes with higher QHE filling factors ν can be supported in our model. Here we show the example for $\nu = 2$ for which there are two hinge modes per surface, see Fig. 14.

APPENDIX C: BAND STRUCTURE OF INFINITE SYSTEM

For chosen in the main text periodicity of the CDW potential $k_w = \pi/4$, the effective unit cell contains four different sites denoted by index $\sigma = 1, 2, 3, 4$, with corresponding creation operators of particle in the nth unit cell denoted by $c^\dagger_{n,\sigma}$. The Hamiltonian of the single 1D CDW modulated wire in momentum space can be found by applying Fourier transform: $c_{n,\sigma} = \frac{1}{\sqrt{N_x}} \sum_{k_x} c_{k_x,\sigma} e^{-ina_x k_x}$, which gives:

$$H^{1D}_{\mathrm{CDW}} = \sum_{k_x} \Psi^\dagger \begin{pmatrix} -\mu - 2U_0\cos(0+\varphi) & -t_x & 0 & -t_x e^{ia_x k_x} \\ -t_x & -\mu - 2U_0\cos(\pi/2+\varphi) & -t_x & 0 \\ 0 & -t_x & -\mu - 2U_0\cos(\pi+\varphi) & -t_x \\ -t_x e^{-ia_x k_x} & 0 & -t_x & -\mu - 2U_0\cos(3\pi/2+\varphi) \end{pmatrix} \Psi \tag{C1}$$

with $\Psi = (c_{k_x,1}, c_{k_x,2}, c_{k_x,3}, c_{k_x,4})^T$. In Fig. 15, we show the band structure of such a wire in the momentum space as a function of the CDW phase ϕ and momentum k_x. The spectrum consists of four bands. As expected, the bulk gaps are the same as found before in the finite-size modeling.

In order to distinguish which gaps in the spectrum of a finite 3D system are opened by finite-size effects and which are opened by combination of CDW and magnetic field we consider Hamiltonians in the momentum space that correspond to the infinite-size limit. Such Hamiltonians for given parameters $2k_w a_x = \pi/2$ and $\phi = \pi/2$ can be obtained by introducing the unit cell composed of four sites in the x direction and four sites in the y direction and by applying Fourier transforms:

$$H^{3D}_{k_x,k_y,k_z} = \sum_{k_x} \Psi^\dagger_{k_x,k_y,k_z} \begin{pmatrix} H^{(1)}_{k_x,k_z} & T_y & 0 & T_y e^{ia_y k_y} \\ T_y & H^{(2)}_{k_x,k_z} & T_y & 0 \\ 0 & T_y & H^{(3)}_{k_x,k_z} & T_y \\ T_y e^{-ia_y k_y} & 0 & T_y & H^{(4)}_{k_x,k_z} \end{pmatrix} \Psi_{k_x,k_y,k_z}, \tag{C2}$$

with

$$H^{(m)}_{k_x,k_z} = \begin{pmatrix} H^{(m)}_1(k_z,\varphi) & -t_x & 0 & -t_x e^{ia_x k_x} \\ -t_x & H^{(m)}_2(k_z,\varphi) & -t_x & 0 \\ 0 & -t_x & H^{(m)}_3(k_z,\varphi) & -t_x \\ -t_x e^{-ia_x k_x} & 0 & -t_x & H^{(m)}_4(k_z,\varphi) \end{pmatrix}, \; T_y = \begin{pmatrix} -t_y & 0 & 0 & 0 \\ 0 & -t_y & 0 & 0 \\ 0 & 0 & -t_y & 0 \\ 0 & 0 & T_y & -t_y \end{pmatrix}, \tag{C3}$$

where

$$H^{(m)}_n(k_z,\varphi) = -\mu - 2U_0\cos(n\pi/2+\varphi) - 2t_z\cos(m\pi/2 + k_z a_z).$$

The corresponding energy spectrum $E(\mathbf{k})$ is presented in the main text [see Fig. 6(a)], demonstrating the 3D bulk character of energy gaps.

[1] K. V. Klitzing, G. Dorda, and M. Pepper, Phys. Rev. Lett. **45**, 494 (1980).

[2] D. C. Tsui, H. L. Stormer, and A. C. Gossard, Phys. Rev. Lett. **48**, 1559 (1982).

[3] R. E. Prange and S. M. Girvin, *The Quantum Hall Effect* (Springer, New York, 1990).

[4] A. H. McDonald, *Quantum Hall Effect: A Perspective* (Kluwer Academic Publishing, Boston, Dordrecht, 1990).

[5] D. J. Thouless, M. Kohmoto, M. P. Nightingale, and M. den Nijs, Phys. Rev. Lett. **49**, 405 (1982).

[6] R. B. Laughlin, Phys. Rev. Lett. **50**, 1395 (1983).

[7] J. K. Jain, Phys. Rev. Lett. **63**, 199 (1989).

[8] X.-L. Qi and S.-C. Zhang, Rev. Mod. Phys. **83**, 1057 (2011).
[9] W. A. Benalcazar, J. C. Y. Teo, and T. L. Hughes, Phys. Rev. B **89**, 224503 (2014).
[10] W. A. Benalcazar, B. A. Bernevig, and T. L. Hughes, Science **357**, 61 (2017).
[11] W. A. Benalcazar, B. A. Bernevig, and T. L. Hughes, Phys. Rev. B **96**, 245115 (2017).
[12] Z. Song, Z. Fang, and C. Fang, Phys. Rev. Lett. **119**, 246402 (2017).
[13] Y. Peng, Y. Bao, and F. von Oppen, Phys. Rev. B **95**, 235143 (2017).
[14] S. Imhof, C. Berger, F. Bayer, H. Brehm, L. Molenkamp, T. Kiessling, F. Schindler, C. H. Lee, M. Greiter, T. Neupert, and R. Thomale, Nat. Phys. **14**, 925 (2018).
[15] J. Langbehn, Y. Peng, L. Trifunovic, F. von Oppen, and P. W. Brouwer, Phys. Rev. Lett. **119**, 246401 (2017).
[16] M. Geier, L. Trifunovic, M. Hoskam, and P. W. Brouwer, Phys. Rev. B **97**, 205135 (2018).
[17] F. Schindler, A. M. Cook, M. G. Verginory, Z. Wang, S. S. P. Parking, B. A. Bernevig, and T. Neupert, Sci. Adv. **4**, eaat0346 (2018).
[18] C.-H. Hsu, P. Stano, J. Klinovaja, and D. Loss, Phys. Rev. Lett. **121**, 196801 (2018).
[19] M. Ezawa, Phys. Rev. B **97**, 155305 (2018).
[20] M. Ezawa, Sci. Rep. **9**, 5286 (2019).
[21] M. Ezawa, Phys. Rev. Lett. **121**, 116801 (2018).
[22] X. Zhu, Phys. Rev. B **97**, 205134 (2018).
[23] Q. Wang, C.-C. Liu, Y.-M. Lu, and F. Zhang, Phys. Rev. Lett. **121**, 186801 (2018).
[24] S. H. Kooi, G. van Miert, and C. Ortix, Phys. Rev. B **98**, 245102 (2018).
[25] Z. Yan, F. Song, and Z. Wang, Phys. Rev. Lett. **121**, 096803 (2018).
[26] T. Liu, J. J. He, and F. Nori, Phys. Rev. B **98**, 245413 (2018).
[27] X. Zhang, H.-X. Wang, Z.-K. Lin, Z. Tian, B. Xie, M.-H. Lu, Y.-F. Chen, and J.-H. Jian, Nat. Phys. **15**, 582 (2019).
[28] Q. Wang, D. Wang, and Q.-H. Wang, Europhys. Lett. **124**, 50005 (2018).
[29] Y. Volpez, D. Loss, and J. Klinovaja, Phys. Rev. Lett. **122**, 126402 (2019).
[30] L. Trifunovic and P. W. Brouwer, Phys. Rev. X **9**, 011012 (2019).
[31] R. J. Slager, L. Rademaker, J. Zaanen, and Leon Balents, Phys. Rev. B **92**, 085126 (2015).
[32] W. A. Benalcazar, T. Li, and T. H. Hughes, Phys. Rev. B **99**, 245151 (2019).
[33] S. A. A. Ghorashi, X. Hu, T. L. Hughes, and E. Rossi, Phys. Rev. B **100**, 020509(R) (2019).
[34] N. Bultinck, B. A. Bernevig, and M. P. Zaletel, Phys. Rev. B **99**, 125149 (2019).
[35] S. H. Kooi, G. van Miert, and C. Ortix, Phys. Rev. B **102**, 041122 (2020).
[36] G. Montambaux and M. Kohmoto, Phys. Rev. B **41**, 11417 (1990).
[37] M. Kohmoto, B. I. Halperin, and Y.-S. Wu, Phys. Rev. B **45**, 13488 (1992).
[38] Z. Kunszt and A. Zee, Phys. Rev. B **44**, 6842 (1991).
[39] M. Koshino, H. Aoki, K. Kuroki, S. Kagoshima, and T. Osada, Phys. Rev. Lett. **86**, 1062 (2001).
[40] M. Koshino and H. Aoki, Phys. Rev. B **67**, 195336 (2003).
[41] M. Koshino, H. Aoki, and B. I. Halperin, Phys. Rev. B **66**, 081301(R) (2002).
[42] M. Koshino and H. Aoki, Phys. Rev. B **69**, 081303(R) (2004).
[43] A. Zamora, G. Szirmai, and M. Lewenstein, Phys. Rev. A **84**, 053620 (2011).
[44] Y. Li, Phys. Rev. B **91**, 195133 (2015).
[45] F. Tang, Y. Ren, P. Wang, R. Zhong, J. Schneeloch, S. A. Yang, K. Yang, P. A. Lee, G. Gu, Z. Qiao, and L. Zhang, Nature (London) **569**, 537 (2019).
[46] A. Lebed, ZhETF Pisma Redaktsiiu **43**, 137 (1986).
[47] V. M. Yakovenko, Phys. Rev. B **43**, 11353 (1991).
[48] J. Klinovaja and D. Loss, Phys. Rev. Lett. **111**, 196401 (2013).
[49] J. C. Y. Teo and C. L. Kane, Phys. Rev. B **89**, 085101 (2014).
[50] J. Klinovaja and Y. Tserkovnyak, Phys. Rev. B **90**, 115426 (2014).
[51] I. Seroussi, E. Berg, and Y. Oreg, Phys. Rev. B **89**, 104523 (2014).
[52] E. Sagi and Y. Oreg, Phys. Rev. B **90**, 201102 (2014).
[53] T. Meng and E. Sela, Phys. Rev. B **90**, 235425 (2014).
[54] J. Klinovaja, Y. Tserkovnyak, and D. Loss, Phys. Rev. B **91**, 085426 (2015).
[55] T. Meng, T. Neupert, M. Greiter, and R. Thomale, Phys. Rev. B **91**, 241106 (2015).
[56] P. Szumniak, J. Klinovaja, and D. Loss, Phys. Rev. B **93**, 245308 (2016).
[57] M. Thakurathi, J. Klinovaja, and D. Loss, Phys. Rev. B **98**, 245404 (2018).
[58] T. Meng, Eur. Phys. J. Special Topics **229**, 527 (2020).
[59] T. Giamarchi, *Quantum Physics in One Dimension* (Oxford University Press, Oxford, 2004).
[60] J. Klinovaja and D. Loss, Eur. Phys. J. B **87**, 171 (2014).
[61] K. S. Bedell, in *Strongly Correlated Electronic Materials: The Los Alamos Symposium 1993*, edited by K. S. Bedell (Addison, Wesley, 1994), pp. 15–18.
[62] R. E. Algra, M. A. Verheijen, M. T. Borgstrom, L. F. Feiner, G. Immink, W. J. van Enckevort, E. Vlieg, and E. P. Bakkers, Nature (London) **456**, 369 (2008).
[63] R. A. Deutschmann, W. Wegscheider, M. Rother, M. Bichler, G. Abstreiter, C. Albrecht, and J. H. Smet, Phys. Rev. Lett. **86**, 1857 (2001).
[64] S. Gangadharaiah, L. Trifunovic, and D. Loss, Phys. Rev. Lett. **108**, 136803 (2012).
[65] J.-H. Park, G. Yang, J. Klinovaja, P. Stano, and D. Loss, Phys. Rev. B **94**, 075416 (2016).
[66] C. W. Groth, M. Wimmer, A. R. Akhmerov, and X. Waintal, New J. Phys. **16**, 063065 (2014).
[67] S. Pandey and C. Ortix, Phys. Rev. B **93**, 195420 (2016).
[68] I. Tamm, Phys. Z. Sowjetunion **1**, 733 (1932).
[69] A. W. Maue, Z. Phys. **94**, 717 (1935).
[70] W. Shockley, Phys. Rev. **56**, 317 (1939).
[71] P. G. Harper, Proc. Phys. Soc. London, Sect. A **68**, 874 (1955).
[72] S. Aubry and G. Andre, Ann. Isr. Phys. Soc. **3**, 133 (1980).
[73] J.-W. Rhim, J. Behrends, and J. H. Bardarson, Phys. Rev. B **95**, 035421 (2017).
[74] G. van Miert and C. Ortix, Phys. Rev. B **96**, 235130 (2017).

[75] M. Pletyukhov, D. M. Kennes, J. Klinovaja, D. Loss, and H. Schoeller, Phys. Rev. B **101**, 165304 (2020); **101**, 161106(R) (2020).
[76] M. Pletyukhov, D. M. Kennes, K. Piasotski, J. Klinovaja, D. Loss, and H. Schoeller, Phys. Rev. Research **2**, 033345 (2020).
[77] L. Fu and C. L. Kane, Phys. Rev. B **76**, 045302 (2007).
[78] H. C. Po, A. Vishwanath, and H. Watanabe, Nat. Commun. **8**, 50 (2017).
[79] D. R. Hofstadter, Phys. Rev. B **14**, 2239 (1976).
[80] C. L. M. Wong, J. Liu, K. T. Law, and P. A. Lee, Phys. Rev. B **88**, 060504(R) (2013).
[81] A. Daido and Y. Yanase, Phys. Rev. B **95**, 134507 (2017).
[82] Y. Volpez, D. Loss, and J. Klinovaja, Phys. Rev. B **97**, 195421 (2018).
[83] K.-I. Imura, M. Okamoto, Y. Yoshimura, Y. Takane, and T. Ohtsuki, Phys. Rev. B **86**, 245436 (2012).
[84] H. Ozawa, A. Yamakage, M. Sato, and Y. Tanaka, Phys. Rev. B **90**, 045309 (2014).
[85] M. Okamoto, Y. Takane, and K.-I. Imura, Phys. Rev. B **89**, 125425 (2014).
[86] K. Kobayashi, H. Satsukawa, J. Yamada, T. Terashima, and S. Uji, Phys. Rev. Lett. **112**, 116805 (2014).
[87] M. Lewenstein, A. Sanpera, V. Ahufinger, B. Damski, A. Sen, and U. Sen, Adv. Phys. **56**, 243 (2007).
[88] M. Aidelsburger, M. Atala, M. Lohse, J. T. Barreiro, B. Paredes, and I. Bloch, Phys. Rev. Lett. **111**, 185301 (2013).
[89] M. Aidelsburger, M. Lohse, C. Schweizer, M. Atala, J. T. Barreiro, S. Nascimbene, N. Cooper, I. Bloch, and N. Goldman, Nat. Phys. **11**, 162 (2015).
[90] Y. E. Kraus, Y. Lahini, Z. Ringel, M. Verbin, and O. Zilberberg, Phys. Rev. Lett. **109**, 106402 (2012).
[91] D. Rainis, A. Saha, J. Klinovaja, L. Trifunovic, and D. Loss, Phys. Rev. Lett. **112**, 196803 (2014).
[92] C. W. Hsu, B. Zhen, A. D. Stone, J. D. Joannopoulos, and M. Soljacic, Nat. Rev. Mater. **1**, 16048 (2016).
[93] F. Ronetti, K. Plekhanov, D. Loss, and J. Klinovaja, Phys. Rev. Research **2**, 022052 (2020).
[94] T. Meng, P. Stano, J. Klinovaja, and D. Loss, Eur. Phys. J. B **87**, 203 (2014).